Bone 127 (2019) 503–509

Contents lists available at ScienceDirect

Bone

journal homepage: www.elsevier.com/locate/bone

Full Length Article

A rare *TTC30B* variant is identified as a candidate for synpolydactyly in a Chinese pedigree

Ye Du[a,b], Fangfang Chen[b], Jian Zhang[c], Zheguang Lin[b], Qian Ma[b], Guisheng Xu[c], Deming Xiao[c], Yaoting Gui[b], Jun Yang[d,*], Shengxiang Wan[c,*]

[a] Medical Research Center, The People's Hospital of Longhua, Shenzhen 518109, China
[b] Guangdong Key Laboratory of Male Reproductive Medicine and Genetics, Peking University Shenzhen Hospital, Shenzhen 518036, China
[c] Department of Hand Microsurgery, Peking University Shenzhen Hospital, Shenzhen 518036, China
[d] Department of Radiology, Peking University Shenzhen Hospital, Shenzhen 518036, China

ARTICLE INFO

Keywords:
Synpolydactyly
TTC30B
Exome sequencing
Shh signaling pathway
Intraflagellar transport

ABSTRACT

Background: Syndactyly type II (synpolydactyly, SPD) is a rare autosomal dominant inherited disease with higher incomplete penetrance. Currently, several variants in *HOXD13* and one deletion in *FBLN1* have been associated with SPD. However, the causative variants in several SPD families and their etiological mechanism are still largely unknown.

Methods: Whole exome and PCR-sanger sequencing followed by two-point linkage analysis were performed to identify the pathogenic variant in a six-generation Chinese pedigree. Homology modeling in combination with the RNAi and qRT-PCR experiments was used for revealing the pathogenic mechanism of the *TTC30B* variant.

Results: A six-generation SPD family was reported. The affected subjects in this family had no other clinical malformation beyond SPD. A rare missense variant c.1157C > T [p.Ala375Val] (chr2:178416368, hg19) in *TTC30B* was demonstrated to be responsible for this SPD family. The modeling structure indicated that the Ala375 was evolutionarily and structurally conserved. The variant p.Ala375Val was predicted to be deleterious for protein structure and/or stability. Two-point linkage analysis resulted in a maximum LOD score of 3.1444 (P = 0.000071). Furthermore, we found that *TTC30B* was regulated by the Shh signaling pathway and the abnormal expression of *TTC30B* will affect the activation of the Shh signaling pathway in human retinal pigment epithelial cells.

Conclusions: This study demonstrates for the first time that an IFT (intraflagellar transport) - related gene *TTC30B* is implicated with SPD.

1. Introduction

Syndactyly type II (synpolydactyly, SPD) is characterized by bilateral webbing between 3/4 fingers and between 4/5 toes with partial or complete digital duplication within the syndactylous web [1]. As an autosomal dominant inherited disease, SPD depicts higher incomplete penetrance (estimated from 86% to 97%) [2] with variable and asymmetrical expressivity [1]. Therefore, the broad spectrum of inter- and intra-familial clinical variability within SPD and overlapping phenotypic manifestations with other subtypes can confuse the clinical classification and further diagnosis. To date, three genetically distinct synpolydactyly types are designated as SPD1, SPD2 and SPD3. SPD1 (MIM: 186000) is the most frequent subtype, caused by heterozygous or homozygous mutations of the *HOXD13* gene on chromosome 2q31 [3]. SPD2 (MIM: 608180), which has been described in only one family, is caused by disruption of the *FBLN1* gene on chromosome 22q13.31 [4]. SPD3 (MIM: 610234), segregating in a large Pakistani kindred, is approximately associated with the 20.54 cM region on chromosome 14q11.2-q12 [5]. However, the pathogenic mutations in several SPD families were underdetermined and some novel causative mutations (i.e. *GLI3*:c.480dupC) were not still covered by this classification system [6].

HOXD13 belongs to a large family of homeobox transcription factors and has been proven to play an important role during embryonic pattern formation [3,7]. Sonic hedgehog (Shh) functions as the major morphogen in patterning the anteroposterior axis of future limbs and digital development [8–10]. *HOXD13* and other 5′ *HOX* genes are shown to be the direct targets of the Shh signaling pathway [11].

* Corresponding authors at: Peking University Shenzhen Hospital, Shenzhen 518036, China.
E-mail addresses: ayjayj_44@163.com (J. Yang), sxwan620328@sina.com (S. Wan).

https://doi.org/10.1016/j.bone.2019.07.012
Received 27 May 2019; Received in revised form 2 July 2019; Accepted 11 July 2019
Available online 12 July 2019
8756-3282/ © 2019 Elsevier Inc. All rights reserved.

Considerable evidence has suggested that the Shh signaling pathway is a cilia-mediated and IFT (intraflagellar transport) -based process [12–14]. The pivotal role of the Shh pathway and IFT process in limb development is supported by the findings that mutations leading to defective Shh signaling and abnormal IFT also result in either abnormal digital numbers or changes in digital identity [15]. Alternatively, genetic mutations in Shh- or IFT-related genes usually lead to more severe multiorgan syndromes [16,17].

In this study, we describe a six-generation Chinese SPD pedigree and identified a novel pathogenic variant in *TTC30B* using exome sequencing in combination with two-point linkage analysis. We also explored the possible pathogenic mechanism through investigating the structure and function of TTC30B protein.

2. Methods

2.1. Ethical approval and sample characterization

This study was approved by Peking University Shenzhen Hospital Review Board Ethics Committee (Shenzhen, China.). A six-generation Chinese family with SPD was recruited in Guangdong province, south of China. Informed consent was obtained from all participants or their legal guardians/parents. Permission was also gained to use their data and pictures for publishing. A pedigree was constructed to draw the relationship and the disease status. Blood samples from twenty subjects including 9 healthy and 11 affected subjects were collected. DNA from 6 family members (4 affected and 2 healthy individuals) was subjected to exome sequencing.

2.2. Genomic DNA extraction and exome sequencing

Subjects were sequenced in collaboration with the BGI at Shenzhen. Briefly, genomic DNA was extracted and further purified from peripheral blood leukocytes using the QIAamp DNA Mini kit according to the manufacturer's protocols (QIAGEN, Hilden, Germany). The qualified genomic DNA sample was randomly fragmented by focused ultrasonicator (Covaris, Woburn, MA, USA), and the size of the library fragments was mainly distributed between 200 and 250 bp. Then adapters were ligated to both ends of the resulting fragments. The adapter-ligated DNA were purified by AMPure SPRI beads (Agencourt, Sugar Land, TX, USA), and fragments with an insert size of approximately 250 bp were excised. Extracted DNA was amplified by ligation-mediated PCR, purified, and hybridized to the SureSelect Biotinylated RNA Library (Agilent Technologies, Santa Clara, CA, USA) for enrichment. Hybridized fragments were bound to strepavidin beads whereas nonhybridized fragments were washed out after 24 h. Captured LM-PCR products were analyzed by an Agilent 2100 Bioanalyzer (Agilent Technologies, Santa Clara, CA, USA) to estimate the magnitude of enrichment. Each captured library was then sequenced on a HiSeq2000 platform (Illumina, San Diego, CA, USA). The sequencing datasets generated and analyzed during the current study are available in the GenBank database under accession number SRP153769 and Genome Sequence Archive database under accession number CRA000972. The other data used in the current study are available from the corresponding author on reasonable request.

2.3. Variants calling, filtration and prioritization

The paired-end 90-bp short reads were mapped onto the UCSC hg19 human reference genome, by SOAPaligner (v2.21) for Single Nucleotide Variant (SNV) calling or by BWA (v0.7.12) for small Insertion/Deletion (InDel) calling. Only uniquely mapped reads were used for coverage and depth calculation and subsequent analysis. The SOAPsnp (v1.03) was used to call high confident genotypes with 2 filter criteria: (1) Phred-like quality of at least 20 and at least 8× coverage for the homozygous genotype or 4× coverage for the heterozygous genotype;

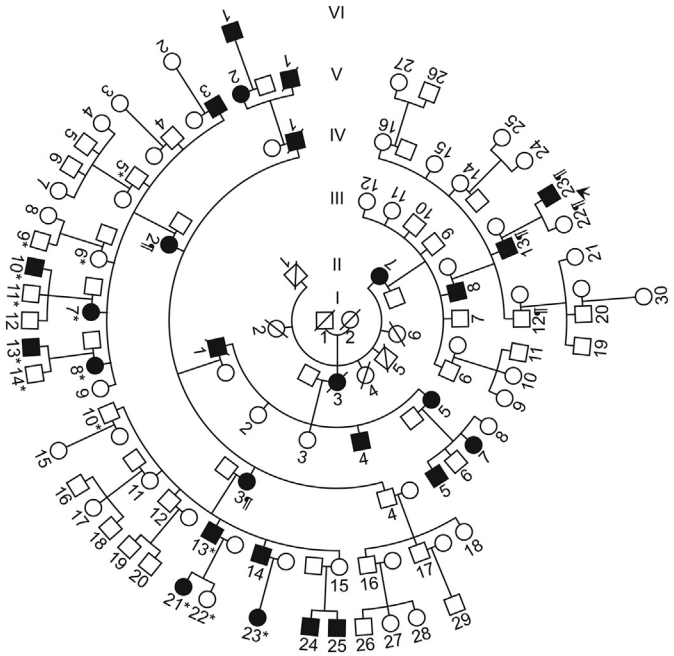

Fig. 1. Pedigree of the Chinese kindred with SPD.
Circles indicate female family members, and squares indicated male family members. Black symbols designate affected individuals, and unfilled symbols designated individuals without SPD. The arrow indicates the proband. The asterisk symbols and the pilcrow symbols indicate the twenty subjects who were clinically examined and sequenced by the PCR-Sanger sequencing method. The pilcrow symbols indicate subjects who were also sequenced by exome sequencing.

(2) Consensus genotype with a quality score of at least 20. The Genome Analysis Toolkit (GATK, v3.5) was used to recalibrate the alignments and to call InDels.

After SNVs and InDels were identified, reference gene annotation was performed using in-house software AnnoDB. Four public databases including the 1000 Genomes Project, dbSNP, HapMap and ExAC databases were used for database annotation. Functionality and conservation prediction of SNVs were performed using different databases or methods including SIFT (URL: http://sift.bii.a-star.edu.sg/), PolyPhen-2 (URL: http://genetics.bwh.harvard.edu/pph2/), GERP 2 (URL: http://mendel.stanford.edu/), Mutation assessor (v3, URL: http://mutationassessor.org/) and FATHMM (v2.3, URL: http://fathmm.biocompute.org.uk/). Based on various variant annotation, the suspected causative variants were obtained by SNV filtration using the following criteria: (1) dominant model: heterozygous in four affected subjects, but homozygous reference in two healthy subjects; (2) nonsynonymous variants; (3) the minor allele frequency (MAF) of variants in four public databases was < 0.1%; (4) the variants were predicted as deleterious by two of the four prediction methods mentioned above.

2.4. Variant validation and linkage analysis

To further validate the candidate variant, we sequenced twenty family subjects of whom the peripheral blood samples were previously collected. Based on the genotype results (Table S1), we further performed a two-point linkage analysis using Pseudomarker v2.0 program with the default parameters of dominant mode of inheritance [18]. The P-value of linkage was calculated and then transformed to a maximum LOD score. The combined effects of linkage and linkage disequilibrium were also estimated.

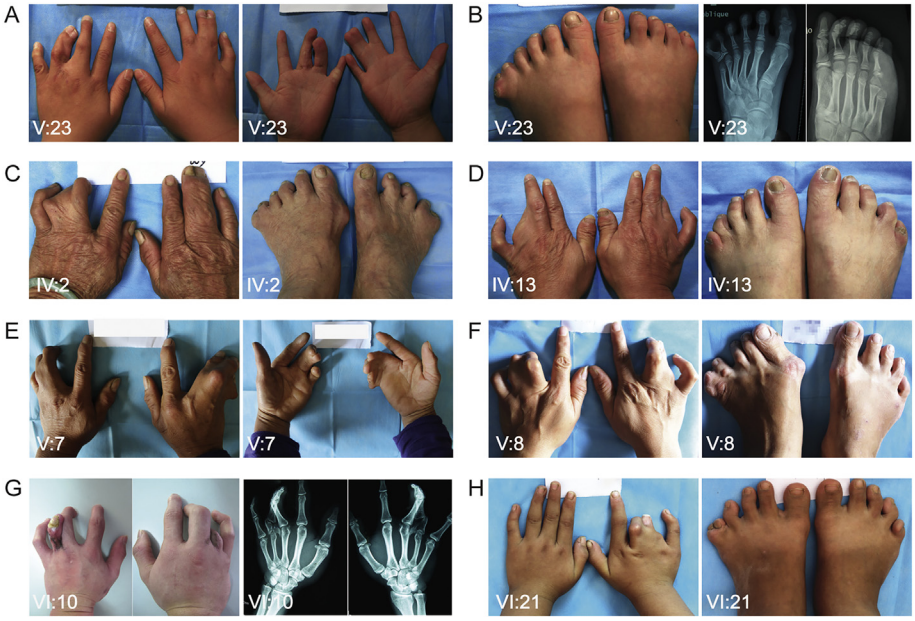

Fig. 2. Clinical photographs and radiographs showing the SPD phenotype in the Chinese family.
(A and B) individual V:23, the proband. (C) individual IV:2. (D) individual IV:13. (E) individual V:7. (F) individual V:8. (G) individual VI:10. (H) individual VI:21.

2.5. Structure modeling and sequence analysis

SWISS-MODEL (URL: https://swissmodel.expasy.org/) was used for protein structure homology-modeling. Structure was colored and labeled using PyMOL software (v2.3, URL: https://pymol.org/2/). SNPeffect (v4.0, URL: http://snpeffect.switchlab.org/) was used to predict the effect of variant. Sequence alignment was performed using MegAlign method in DNAstar software package.

2.6. RNAi, SAG-treatment and real time quantitative PCR assay

The TTC30B-specific siRNA (sense: 5′-GCAUAUCGCUGAGAUUAU UTT-3′) and 6-FAM labeled negative control (NC) was designed and synthesized by GenePharma company (Shanghai, China). The human retinal pigment epith17elial (RPE) cells were cultured in Dulbecco's Modified Eagle's Medium (DMEM) supplemented with 10% (v/v) fetal bovine serum and antibiotics (100 U/ml penicillin, 100 g/ml streptomycin) (Thermo Fisher Scientific, Waltham, MA, USA). For RNAi experiment, confluent RPE cultures was transiently transfected with 100 pmol siRNA or NC siRNA using lipofectamine RNAiMAX transfection reagent (Thermo Fisher Scientific, Waltham, MA, USA). The transfection efficiency was evaluated by counting the number of RPE cells with FAM fluorescence. After 24 h, RPE cultures transfected with NC siRNA or *TTC30B* siRNA were serum starved for 24 h to induce ciliogenesis and then treated with 100 nM SAG (Sigma-Aldrich, St. Louis, MO, USA) for 24 h to activate the Shh pathway or with DMSO as negative control. Total RNA was isolated using RNAiso Plus kit (TaKaRa, Kusatsu, Japan). Reverse transcription was performed using PrimeScript RT reagent kit (TaKaRa, Kusatsu, Japan) according to the manufacturer's instructions. Equal amounts of cDNA were used as templates for quantitative RT-PCR with SYBR Premix Ex tag II kit (TaKaRa, Kusatsu, Japan) and using LightCycler machine (Roche, Basel, Switzerland). The relative expression levels of genes including *TTC30B*, *PTCH1* and *GLI1* were determined using *GADPH* as internal reference and shown as average ± SD. The reported data were calculated based on three independent repeats. The significant differences between different treated groups were statistically analyzed with two-sample paired *t*-test method.

3. Results

3.1. Clinical presentation

We collected information and samples from a large family in Guangdong province in southern China. The family pedigree included 94 individuals spanning six generations (Fig. 1). Twenty-seven subjects (16 males, 11 females) were clinically affected, four of whom were decreased. Twenty subjects, including eleven affected subjects, were physically examined. Except synpolydactyly, no clinical malformation was observed in other organs. The clinical manifestations of this family showed large inter- and intra-individual phenotypic heterogeneity. According to the clinical classification scheme proposed by Malik S. [1], eight of eleven subjects had typical SPD features, represented by cutaneous/bony fusion of 3/4 fingers with or without an extra digit, and cutaneous/bony fusion of 4/5 toes with or without an extra postaxial toe (Fig. 2). Some subjects showed anomalies of metacarpal and metatarsal bones. In three subjects, two had normal hands and one had partially cutaneous webbing of 3/4 fingers only in the right hand. In addition to the typical features, several milder phenotypes, including webbing of 3/4 fingers, clinodactyly of the fifth finger and brachydactyly, were concurrent with typical phenotypes in some subjects. Furthermore, two rare and milder phenotypic manifestations (hallux valgus and torsion of the central axis of the fifth toe) were observed in the unilateral foot in two subjects. Therefore, with the exception of rare clinical features, the clinical manifestations of this family largely overlapped with that of several SPD1 families. The detailed clinical manifestations were summarized in Table S1. Furthermore, the subject V:15 apparently represents a “skipped generation.” Available evidence indicated that she and her husband had no clinical manifestations of syndactyly or polydactyly, but they had two affected sons. Because they had previously moved away, we were unable to contact them and collect further clinical information. Besides, no other case of non-penetrance was observed in this pedigree.

3.2. Identification of the causative variant

Exome sequencing in six family subjects followed by prioritization analysis (Table S2) identified one possibly causative variant (c.1157C > T [p.Ala375Val]; chr2:178416368, hg19) in *TTC30B*

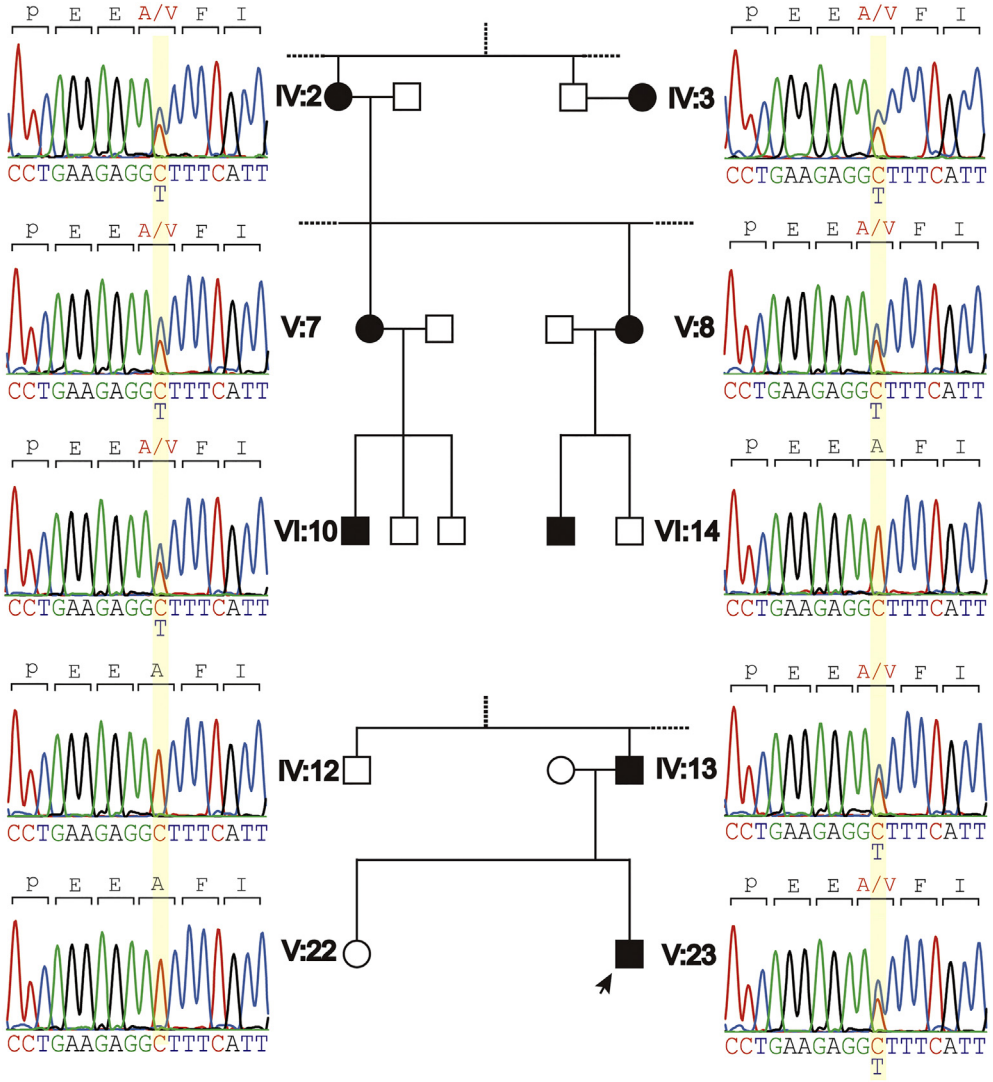

Fig. 3. Variant validation in other family members by PCR-Sanger sequencing. The chromatograms of PCR-Sanger sequencing in several representative subjects are shown.

(tetratricopeptide repeat protein 30B, RefSeq NM_152517.2, located at chromosome 2q31.2). This variant is denoted as rs185026370 in the dbSNP database and has never been associated with any disease or clinical phenotype. The minor allele frequency is 9.18×10^{-4} in the dbSNP and 7.43×10^{-5} in the ExAC database, suggesting that it is a very rare variant. In order to further validate that this variant is responsible for the SPD, we investigated the state of this variant in twenty family members including eleven affected and nine healthy subjects by PCR-Sanger sequencing method. The results revealed that all the affected subjects were heterozygous carriers and the healthy subjects were genotyped as homologous reference (Fig. 3, Table S1). This was also consistent with the autosomal dominant inheritance model of this SPD family. Furthermore, we performed a two-point linkage analysis based on the *TTC30B* variant genotype of twenty subjects (Table S1) using *Pseudomarker* program. Under dominant mode of inheritance, the results showed the P-value of 0.000071 and the maximum LOD of 3.1444. Compared to other commonly used linkage analysis software, *Pseudomarker* is powerful for estimation of the combined effects of linkage and linkage disequilibrium. In this study, the combined effects had a P-value of 0.000009, which is highly significant and firmly supports the linkage. Besides, we did not observe any pathogenic or likely pathogenic variants in the limb-development and syndactyly related genes listed in Table S3.

3.3. *TTC30B c.1157C > T is structurally and evolutionarily conserved*

Homology modeling on the TTC30B protein was performed, using the structure of *Chlamydomonas reinhardtii* ortholog IFT70 (PDB: 4uzy) as template (Fig. 4a). The sequence identity was up to 59% with 95% coverage. Consistent with IFT70, the 2.48-Å modeling structure revealed that TTC30B consisted of 15 consecutive TPRs (tetratricopeptide repeats), which formed 270° of a super helical structure.

From a closer inspection on the structure, the Ala375 was located on the 10th TPR (Fig. 4b). In the TPR motif, the comparatively conserved residues only appear at a few positions (e.g., Gly or Ala at position 8 and Ala at position 20 and 27). The other conserved positions prefer residues with small or aromatic side chains rather than specific residues. Based on the motif alignment results, the Ala375 corresponds to conserved position 20, and the Ala364 corresponds to position 8. These two positions, with a strong preference for small amino acids, are positioned where helices are in close contact. Additionally, the Leu379 and Leu382 correspond to two other conserved positions 24 and 27, respectively. When the Ala375 is mutated to valine (Fig. 4c), the relatively bulky side chain of valine is not tolerated. The SNPeffect prediction results also showed a 3.8 kcal·mol^{-1} increase in folding free energy for the mutant protein, suggesting significantly reduced protein stability. We also assessed the conservation of the primary sequence of

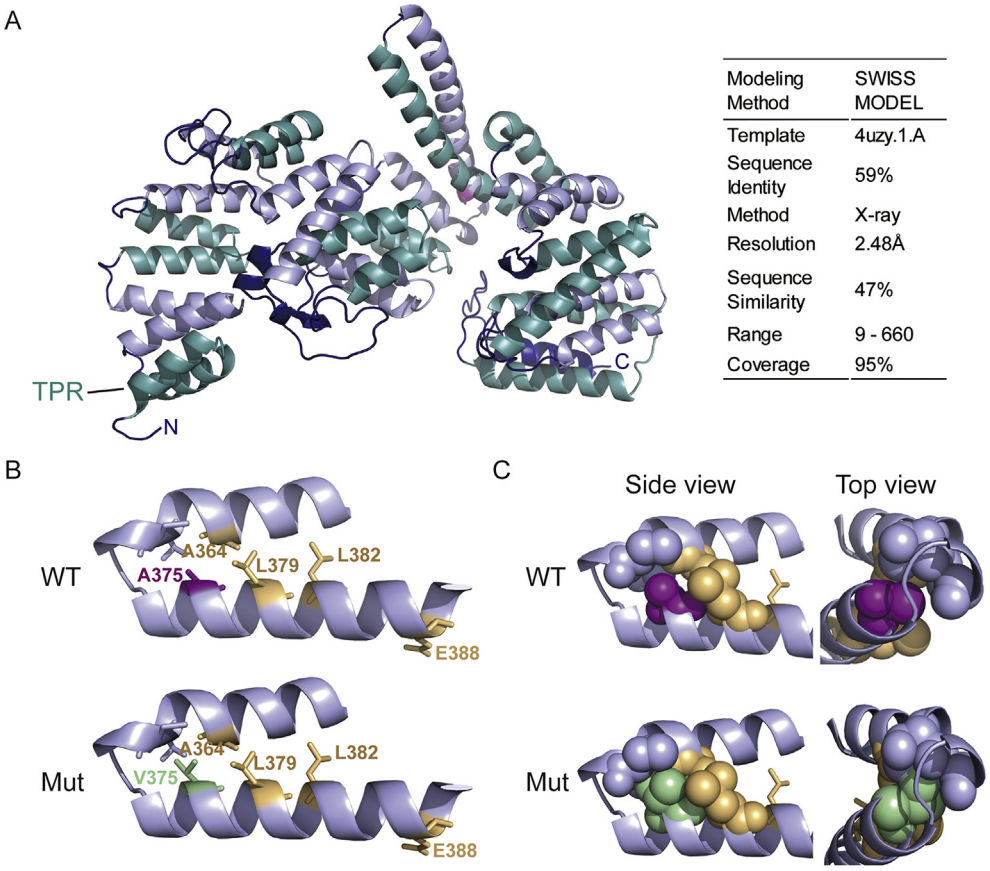

Modeling Method	SWISS MODEL
Template	4uzy.1.A
Sequence Identity	59%
Method	X-ray
Resolution	2.48Å
Sequence Similarity	47%
Range	9 - 660
Coverage	95%

Fig. 4. Structural modeling and Ala375 conservation analysis.
(A) Ribbon representation (left) and parameters (right) of homology modeling structure of TTC30B by SWISS-MODEL. The p.Ala375Val is indicated as light magenta. The 15 TPRs are indicated as light blue and light teal, and the other is in blue.
(B) Cartoon representation of part of the 10th TPR with Ala375 (light magenta) or Val375 (pale green) and several flanking conserved residues (light orange) shown as sticks.
(C) Sphere representation of residues encompassing Ala375 (light magenta) or Val375 (pale green). Compared to the structure of wild type TPR (top), the crowded model of the mutant (bottom) indicate that it is impossible for the alanine to be substituted by valine without disrupting the overall structure because of the steric hindrance.
(D) Multiple sequence alignment of the TPR motif containing Ala375 of TTC30B from diverse species. Ala375 was indicated in red. (For interpretation of the references to colour in this figure legend, the reader is referred to the web version of this article.)

TTC30B with the homologous proteins from different species. The Ala375 was one of the most conserved amino acids (Fig. 4d). Therefore, it is reasonable to suppose that the p.Ala375Val mutation maybe affect the structure and function (or partial function) of TTC30B.

3.4. Abnormal TTC30B affected the SAG-induced activation of the Shh signaling pathway

The Shh signaling pathway plays pivotal role in digit patterning. The IFT system and cilium are essential for the Shh signaling pathway. Therefore, we used RNAi method to inhibit the expression level of *TTC30B* in human RPE (retinal pigment epithelial) cells and used SAG, a small molecule Smoothened agonist, to activate the Shh pathway in vivo. Then we investigate whether the inhibition of *TTC30B* level will affect the activation of Shh signaling pathway. The expression level of two downstream target genes (*PTCH1* and *GLI1*) were selected as indicator of the activation state of the Shh pathway. Our results (Fig. 5) showed a four-fold increase of *PTCH1* and *GLI1* expression and two-fold increase of *TTC30B* in respond to the SAG activation, suggesting that the *TTC30B* was partly regulated by the Shh pathway. But when inhibiting the *TTC30B*, the large up-regulation of *PTCH1* and *GLI1* were affected and the expression level of *TTC30B* was further inhibited.

4. Discussion

In this study, we presented a large Chinese kindred with SPD. Due to the extreme inter- and intra-individual clinical heterogeneity observed in this family and other families associated with *HOXD13* mutations, the clinical manifestations of this family largely overlapped with that of SPD1 families. The pedigree indicated that individual V:15 was suspected to be a nonpenetrant carrier. However, because the subject was unavailable at the time of clinical and molecular examination, the carrier status remains unspecified.

Exome sequencing and PCR-Sanger sequencing demonstrated that a missense variant *TTC30B*:c.1157C > T was responsible for the SPD phenotype in this family. *TTC30B* encoded a TPR motif containing protein. The TPR motif is comprised of 34 amino acid repeats that often form two α-helices. The conservation analysis of the primary sequence and secondary structure revealed a comparatively conserved pattern at eight positions [19]. In this study, the causative variant p.Ala375Val in TTC30B corresponds to the highly conserved position 8, which is the closest position between the two adjacent α-helices [20]. Alanine is among the amino acids with highest propensities in α-helix, while valine strongly prefers forming β-sheet compared to an α-helix [21]. Our modeling structure and prediction results suggest that the structure

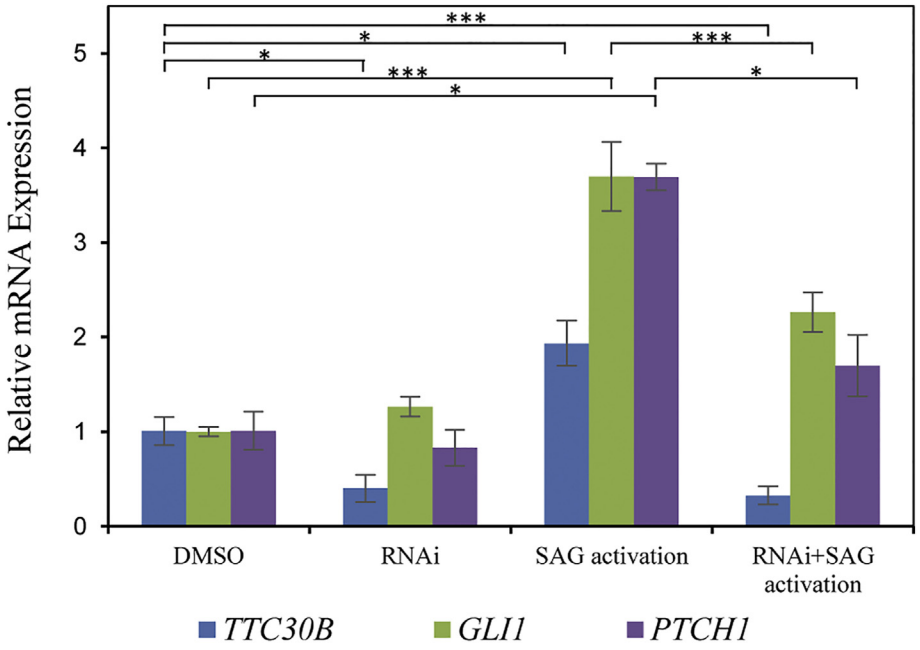

Fig. 5. Regulatory relationships between *TTC30B* and Shh signaling pathway. Quantitative real-time PCR analysis determined the mRNA levels of indicated genes in RPE cells treated with DMSO as negative-control or siRNA targeting *TTC30B* or SAG activating the Shh pathway or siRNA followed by SAG activation. Data are the mean ± SD of three independent experiments. *, $P < 0.05$; ***, $P < 0.01$.

and/or the stability of TTC30B should be affected by p.Ala375val mutation, although more experimental evidence are needed to confirm the conclusion.

The TPR motif is present ubiquitously in proteins and mediates a variety of protein-protein interactions. The homologous modeling structure showed that TTC30B is only composed of TPR motifs, suggesting that its sole function is protein-protein interaction. Although the exact function of *TTC30B* in human is still largely unknown, several studies on its homologous genes in other ciliated organisms (e.g., *Chlamydomonas reinhardtii*, *C. elegans*, etc.) have suggested that the homologous proteins of TTC30B participate in the assembly of IFT-B core complex through directly interacting with other IFT subunits [22,23] and are required for cargos association and/or transport [24–26]. Recently, a study in human RPE cells revealed that *TTC30B* is required for ciliogenesis and dispensable for assembly of the residual IFT-B subunits [27]. In this study, we found that *TTC30B* is up-regulated in response to the activation of the Shh signaling pathway and then the decreased expression of *TTC30B* affects the Shh signaling pathway. It is worthy to note that only 60% of *TTC30B* transcriptions can be inhibited by RNAi method in this study, so the regulatory mechanism between *TTC30B* and the Shh signaling pathway still needs further investigation in the following studies. As mentioned in the Introduction section, the Shh signaling pathway plays a pivotal role in regulating limb development and digit patterning, and the IFT process is essential for the Shh signaling pathway [12]. Thus, we propose that the SPD-causing variant has an impact on the structure of TTC30B and subsequently affects, to some extent, its function in the IFT process and the Shh signaling pathway.

5. Conclusions

In the present study, we reported a novel variant c.1157C > T in *TTC30B* responsible for SPD in a Chinese family. In silico studies suggested that the causative variant may affect the protein structure and/or stability. We further demonstrated that *TTC30B* is regulated by the Shh signaling pathway and its abnormal expression will affect the activation of the Shh signaling pathway. Therefore, considering the pivotal role of *TTC30B* in ciliogenesis, we proposed that *TTC30B*, encoding one core subunit of IFT-B complex, may be responsible for regulating digit patterning through Shh signaling pathway. This study demonstrates for the first time that an IFT-related gene is implicated with SPD and will shed new light on the regulation network in the process of digit patterning and the molecular etiology of SPD.

Supplementary data to this article can be found online at https://doi.org/10.1016/j.bone.2019.07.012.

Declaration of Competing Interest

The authors declare that they have no competing interests.

Acknowledgements

We are most grateful to the family for their participation in our study. We sincerely thank Professor Jurg Ott from Rockefeller University for helps in linkage analysis. This work was supported by National Natural Science Foundation of China [Grant number 81501847] and the Health and Family Planning Commission Project of Shenzhen Municipality, China [Grant number 201606003].

Authors' contributions

YD, YTG, JY and SXW participated in the design of this study and interpretation of data. YD and FFC participated in all the laboratory analyses. JZ and ZGL participated in sample collection, DNA extraction and exome sequencing. QM prepared the figure for protein structure. JZ, GSX and DMX provided patients data. YD drafted this manuscript. JY and SXW gave final approval of the version to be published. All authors read and approved the final version of the final manuscript.

References

[1] S. Malik, K.H. Grzeschik, Synpolydactyly: clinical and molecular advances, Clin. Genet. 73 (2) (2008) 113–120.
[2] A.N. Akarsu, O. Akhan, B.S. Sayli, U. Sayli, G. Baskaya, M. Sarfarazi, A large Turkish kindred with syndactyly type II (synpolydactyly). 2. Homozygous phenotype? J. Med. Genet. 32 (6) (1995) 435–441.
[3] N. Brison, P. Tylzanowski, P. Debeer, Limb skeletal malformations - what the HOX is going on? Eur. J. Med. Genet. 55 (1) (2012) 1–7.
[4] P. Debeer, E.F. Schoenmakers, W.O. Twal, W.S. Argraves, L. De Smet, J.P. Fryns, W.J. Van De Ven, The fibulin-1 gene (FBLN1) is disrupted in a t(12;22) associated with a complex type of synpolydactyly, J. Med. Genet. 39 (2) (2002) 98–104.
[5] S. Malik, A.A. Abbasi, M. Ansar, W. Ahmad, M.C. Koch, K.H. Grzeschik, Genetic heterogeneity of synpolydactyly: a novel locus SPD3 maps to chromosome 14q11.2-q12, Clin. Genet. 69 (6) (2006) 518–524.
[6] R. Kang, S. Huang, J. Li, Y. Zou, P. Xu, M. Gao, L. Wang, H. Xie, J. Yan, Y. Gao, A

novel mutation of GLI3 gene underlying synpolydactyly in a family, Zhonghua Yi Xue Yi Chuan Xue Za Zhi 34 (4) (2017) 490–493.
[7] M.A. Ros, HOX13 proteins: the molecular switcher in Hoxd bimodal regulation, Genes Dev. 30 (10) (2016) 1135–1137.
[8] A. Kicheva, M. Cohen, J. Briscoe, Developmental pattern formation: insights from physics and biology, Science 338 (6104) (2012) 210–212.
[9] B. Wang, J.F. Fallon, P.A. Beachy, Hedgehog-regulated processing of Gli3 produces an anterior/posterior repressor gradient in the developing vertebrate limb, Cell 100 (4) (2000) 423–434.
[10] B.D. Harfe, P.J. Scherz, S. Nissim, H. Tian, A.P. McMahon, C.J. Tabin, Evidence for an expansion-based temporal Shh gradient in specifying vertebrate digit identities, Cell 118 (4) (2004) 517–528.
[11] M. Welten, G. Pavlovska, Y. Chen, Y. Teruoka, M. Fisher, F. Bangs, M. Towers, C. Tickle, 3D expression patterns of cell cycle genes in the developing chick wing and comparison with expression patterns of genes implicated in digit specification, Dev. Dyn. 240 (5) (2011) 1278–1288.
[12] X. Yuan, S. Yang, Cilia/Ift protein and motor -related bone diseases and mouse models, Front. Biosci. 20 (2015) 515–555.
[13] J.T. Eggenschwiler, K.V. Anderson, Cilia and developmental signaling, Annu. Rev. Cell Dev. Biol. 23 (2007) 345–373.
[14] D. Huangfu, A. Liu, A.S. Rakeman, N.S. Murcia, L. Niswander, K.V. Anderson, Hedgehog signalling in the mouse requires intraflagellar transport proteins, Nature 426 (6962) (2003) 83–87.
[15] T. Suzuki, How is digit identity determined during limb development? Develop. Growth Differ. 55 (1) (2013) 130–138.
[16] J. Briscoe, P.P. Therond, The mechanisms of Hedgehog signalling and its roles in development and disease, Nat. Rev. Mol. Cell Biol. 14 (7) (2013) 416–429.
[17] L.G. Biesecker, Polydactyly: how many disorders and how many genes? 2010 update, Dev. Dyn. 240 (5) (2011) 931–942.
[18] E.M. Gertz, T. Hiekkalinna, S.L. Digabel, C. Audet, J.D. Terwilliger, A.A. Schaffer, PSEUDOMARKER 2.0: efficient computation of likelihoods using NOMAD, BMC Bioinf. 15 (2014) 47.
[19] F. Parmeggiani, P.S. Huang, S. Vorobiev, R. Xiao, K. Park, S. Caprari, M. Su, J. Seetharaman, L. Mao, H. Janjua, G.T. Montelione, J. Hunt, D. Baker, A general computational approach for repeat protein design, J. Mol. Biol. 427 (2) (2015) 563–575.
[20] G.L. Blatch, M. Lassle, The tetratricopeptide repeat: a structural motif mediating protein-protein interactions, Bioessays 21 (11) (1999) 932–939.
[21] P.Y. Chou, G.D. Fasman, Conformational parameters for amino acids in helical, beta-sheet, and random coil regions calculated from proteins, Biochemistry 13 (2) (1974) 211–222.
[22] M. Taschner, F. Kotsis, P. Braeuer, E.W. Kuehn, E. Lorentzen, Crystal structures of IFT70/52 and IFT52/46 provide insight into intraflagellar transport B core complex assembly, J. Cell Biol. 207 (2) (2014) 269–282.
[23] J.A. Follit, F. Xu, B.T. Keady, G.J. Pazour, Characterization of mouse IFT complex B, Cell Motil. Cytoskeleton 66 (8) (2009) 457–468.
[24] G. Ou, O. E. Blacque, J.J. Snow, M.R. Leroux, J.M. Scholey, Functional coordination of intraflagellar transport motors, Nature 436 (7050) (2005) 583–587.
[25] G. Ou, M. Koga, O.E. Blacque, T. Murayama, Y. Ohshima, J.C. Schafer, C. Li, B.K. Yoder, M.R. Leroux, J.M. Scholey, Sensory ciliogenesis in Caenorhabditis elegans: assignment of IFT components into distinct modules based on transport and phenotypic profiles, Mol. Biol. Cell 18 (5) (2007) 1554–1569.
[26] N. Pathak, T. Obara, S. Mangos, Y. Liu, I.A. Drummond, The zebrafish fleer gene encodes an essential regulator of cilia tubulin polyglutamylation, Mol. Biol. Cell 18 (11) (2007) 4353–4364.
[27] R. Takei, Y. Katoh, K. Nakayama, Robust interaction of IFT70 with IFT52-IFT88 in the IFT-B complex is required for ciliogenesis, Biol Open 7 (5) (2018).